

Emergence of a radio jet in the changing-look AGN 1ES 1927+654

EILEEN T. MEYER,¹ SIBASISH LAHA,^{2,3,4} ONIC I. SHUVO,¹ AGNIVA ROYCHOWDHURY,^{5,1} DAVID A. GREEN,⁶
LAUREN RHODES,⁷ AMELIA M. HANKLA,^{8,9,*} ALEXANDER PHILIPPOV,¹⁰ ROSTOM MBAREK,^{8,9,*} ARI LAOR,¹¹
MITCHELL C. BEGELMAN,¹² DEV R. SADAULA,^{2,3,4} RITESH GHOSH,^{3,2,4,13} GABRIELE BRUNI,¹⁴ FRANCESCA PANESSA,¹⁴
MATTEO GUAINAZZI,¹⁵ EHUD BEHAR,^{11,16} MEGAN MASTERSON,¹⁶ HAOCHEG ZHANG,^{3,2} XIAOLONG YANG,¹⁷
MARK A. GURWELL,¹⁸ GARRETT K. KEATING,^{18,19} DAVID WILLIAMS-BALDWIN,²⁰ JUSTIN D. BRAY,²⁰
EMMANUEL K. BEMPONG-MANFUL,^{20,21} NICHOLAS WRIGLEY,²⁰ STEFANO BIANCHI,²² FEDERICA RICCI,^{22,23}
FABIO LA FRANCA,²² ERIN KARA,¹⁶ MARKOS GEORGANOPOULOS,¹ SAMANTHA OATES,²⁴ MATT NICHOLL,²⁵ MAIN PAL,²⁶
AND S. BRADLEY CENKO^{2,27}

¹*Department of Physics, University of Maryland Baltimore County, 1000 Hilltop Circle Baltimore, MD 21250, USA*

²*Astrophysics Science Division, NASA Goddard Space Flight Center, Greenbelt, MD 20771, USA.*

³*Center for Space Science and Technology, University of Maryland Baltimore County, 1000 Hilltop Circle, Baltimore, MD 21250, USA.*

⁴*Center for Research and Exploration in Space Science and Technology, NASA/GSFC, Greenbelt, Maryland 20771, USA*

⁵*Space Telescope Science Institute, 3700 San Martin Dr, Baltimore, MD 21218, USA*

⁶*Astrophysics Group, Cavendish Laboratory, 19 J.J. Thomson Avenue, Cambridge CB3 0HE, UK*

⁷*Astrophysics, The University of Oxford, Keble Road, Oxford OX1 3RH, UK*

⁸*Joint Space-Science Institute, University of Maryland, College Park, MD 20742, USA*

⁹*Department of Astronomy, University of Maryland, College Park, MD, USA*

¹⁰*Department of Physics, University of Maryland, College Park, MD 20742, USA*

¹¹*Department of Physics, Technion, Haifa 32000, Israel*

¹²*JILA, University of Colorado and National Institute of Standards and Technology, 440 UCB, Boulder, CO 80309-0440, USA.*

¹³*MKHS, Murshidabad, West Bengal, 742401, India.*

¹⁴*INAF – Istituto di Astrofisica e Planetologia Spaziali, Via del Fosso del Cavaliere 100, Roma, 00133, Italy*

¹⁵*European Space Agency (ESA), European Space Research and Technology Centre (ESTEC), Keplerlaan 1, 2201 AZ Noordwijk, The Netherlands*

¹⁶*Department of Physics & Kavli Institute for Astrophysics and Space Research, Massachusetts Institute of Technology, Cambridge, MA 02139, USA*

¹⁷*Shanghai Astronomical Observatory, CAS, 80 Nandan Road, Shanghai 200030, China*

¹⁸*Center for Astrophysics | Harvard & Smithsonian, 60 Garden Street, Cambridge, MA 02138, USA*

¹⁹*Academia Sinica Institute of Astronomy and Astrophysics, 645 North A'ohoku Place, Hilo, HI 96720, USA*

²⁰*Jodrell Bank Centre for Astrophysics, Department of Physics and Astronomy, The University of Manchester, Manchester M13 9PL, UK*

²¹*School of Physics, University of Bristol, Tyndall Avenue, Bristol BS8 1TL, UK*

²²*Dipartimento di Matematica e Fisica, Università degli Studi Roma Tre, via della Vasca Navale 84, I-00146 Roma, Italy*

²³*INAF-Osservatorio Astronomico di Roma, via Frascati 33, 00040 Monteporzio Catone, Italy*

²⁴*Birmingham Institute for Gravitational Wave Astronomy and School of Physics and Astronomy, University of Birmingham, Birmingham B15 2TT, UK*

²⁵*Astrophysics Research Centre, School of Mathematics and Physics, Queens University Belfast, Belfast BT7 1NN, UK*

²⁶*Department of Physics, Sri Venkateswara College, University of Delhi, Benito Juarez Road, Dhaura Kuan, New Delhi – 110021, India*

²⁷*Joint Space-Science Institute, University of Maryland, College Park, MD 20742, USA*

(Received June 27, 2024)

ABSTRACT

We present multi-frequency (5–345 GHz) and multi-resolution radio observations of 1ES 1927+654, widely considered one of the most unusual and extreme changing-look active galactic nuclei (CL-AGN). The source was first designated a CL-AGN after an optical outburst in late 2017 and has since displayed considerable changes in X-ray emission, including the destruction and rebuilding of the X-ray corona in 2019–2020. Radio observations prior to 2023 show a faint and compact radio source not unusual for a radio-quiet AGN. Starting in February 2023, 1ES 1927+654 began exhibiting a radio flare with a steep exponential rise, reaching a peak 60 times previous flux levels, and has maintained this higher level of radio emission for nearly a year. The 5–23 GHz spectrum is broadly similar to gigahertz-peaked radio sources, which are understood to be young radio jets less than ~ 1000 years old. Recent

high-resolution VLBA observations at 23.5 GHz now show resolved extensions on either side of the core, with a separation of ~ 0.14 pc, consistent with a new and mildly relativistic bipolar outflow. A steady increase in the soft X-ray band (0.3–2 keV) concurrent with the radio may be consistent with jet-driven shocked gas, though further observations are needed to test alternate scenarios. This source joins a growing number of CL-AGN and tidal disruption events which show late-time radio activity, years after the initial outburst.

Keywords: Radio AGN – X-ray AGN – Seyfert galaxies – jets – proper motion

1. INTRODUCTION

Recent advances in time-domain studies have led to the identification of new types of extreme variability in active galaxies, popularly called “changing look” active galactic nuclei (CL-AGNs, hereafter). These extreme variations are not only characterized by orders-of-magnitude changes in the optical, UV, and X-ray luminosity of the source but also by an unexpected transition between optical spectral type (Mathur et al. 2018; Trakhtenbrot et al. 2019; Kokubo & Minezaki 2020; Komossa et al. 2020). In the simplest AGN unification framework, those with broad emission lines (type I) are thought to be viewed more face-on, such that the central nucleus is unobscured, while type II AGN are thought to be viewed at higher inclination angles, in which cases an inferred dusty torus obscures the broad-line emitting clouds, resulting in only narrow optical emission lines in the optical spectrum (Antonucci 1993; Bianchi et al. 2012; Ramos Almeida & Ricci 2017). While we have long known that many factors complicate this simple picture (e.g. strength of the central continuum, variations in the amount and distribution of molecular gas and dust), the drastic changes seen in CL-AGNs in such short timescales (a few weeks to months) challenge the simplest form of the AGN unification framework which has generally assumed that such changes occur over far longer timescales.

The AGN 1ES 1927+654 ($z = 0.018$; $368 \text{ pc}''$) is widely considered one of the most unusual and extreme CL-AGN yet discovered (Trakhtenbrot et al. 2019; Ricci et al. 2020, 2021; Masterson et al. 2022; Laha et al. 2022; Ghosh et al. 2023), and is one of the extremely few CL-AGN observed to change in real time. Earlier X-ray and optical observations of 1ES 1927+654 classified it as a “true” or “naked” type II AGN, with no evidence for obscuration by dust along the line of sight to explain the lack of broad emission lines (Boller et al. 2003; Tran et al. 2011). It was first flagged as a transient source of significantly increasing flux by the All-Sky Automated

Survey for Supernovae (ASAS-SN; Shappee et al. 2014) program on 2018 March 3 (ASAS-SN-18el/AT2018zf; Nicholls et al. 2018). In the original discovery paper, Trakhtenbrot et al. (2019) used archival data from the Asteroid Terrestrial-impact Last Alert System (ATLAS; Tonry et al. 2018) to show that the outburst actually began in December 2017 and that the total increase was nearly 5 magnitudes in the V band (a factor of 100 in total flux). An initially nearly featureless optical quasar spectrum began to show increasing broad lines approximately 70–90 days after the peak in the optical band, which occurred in March 2018. The broad line fluxes continued to increase in strength out to roughly 150 days after the continuum peak, and persisted for at least 11 months after the optical flare. This behavior follows the expectations for the illumination of a previously existing broad line region of size $\sim 1\text{--}3$ light-months.

Subsequent to the initial CL outburst, the source has displayed a series of unusually varied states in the X-ray band while showing no change other than a monotonic return to pre-CL values in the optical/UV and general quiescence in the radio (up to the presently reported outburst). After a short period of X-ray emission similar to pre-CL levels, the 2–10 keV hard X-ray emission (i.e. the corona) completely vanished for about 3 months in 2018 before flaring up by a factor 1000 to exceed the Eddington limit for a $10^6 M_{\odot}$ black hole (Ricci et al. 2020), a state it maintained for over a year before dropping back to pre-outburst levels (Ricci et al. 2021; Masterson et al. 2022).

While the initial optical/UV flare and decay timescale appear consistent with a possible tidal disruption event (TDE) in an existing AGN, the X-ray spectral changes are not, including both short and long-term variability and temperature variations for the thermal X-ray component in the first few years after the CL event (Masterson et al. 2022). One possibility is that the CL event was the result of a magnetic flux inversion event in a magnetically arrested disk or MAD (Scepi et al. 2021). This could explain the much shallower UV flux decay than expected under a TDE, the X-ray minimum following the outburst, and the lack of TDE-like spectral

* Neil Gehrels Fellow

features (Laha et al. 2022). Most recently, Ghosh et al. (2023) have reported the emergence of a new bright and soft X-ray component in 1ES 1927+654 (along with an undiminished X-ray corona), which began in late 2022 and continues up to the present epoch. It was this enhanced state which triggered a director’s discretionary time (DDT) request to the Very Long Baseline Array (VLBA) which led to the fortunate timing of much of the radio monitoring presented here.

2. OBSERVATIONS

2.1. Overview of Past and Present Radio Monitoring

The source 1ES 1927+654 has been observed in the radio with the Very Large Array (VLA) and Very Long Baseline Array (VLBA) on only a few occasions prior to the CL event. Perlman et al. (1996) report a flux density of 16 mJy at 6 cm measured by the VLA in CnB hybrid configuration with a resolution of approximately $5''$. Observations with the VLBA taken in 2013 and 2014 (previously published in Laha et al. 2022) are included here for comparison to more recent data. Post-CL event, the source was observed by the VLBA once at C-band in December 2018 and then sporadically with both the VLBA and European VLBI Network (EVN) on 6–12 month timescales from January 2020 by our group and others. This longer-timescale monitoring was primarily motivated by the months-timescale X-ray changes seen by *Swift* and *NICER*, to look for possible correlated radio variability.

While our standard monitoring observations with the VLBA at 5 GHz showed no major change between 2022 March and August (total flux of 6 and 5 mJy, respectively), we made a director’s discretionary time (DDT) request in April 2023 (BR 256) based on the soft X-ray flux seen by *Swift*, which had been steadily rising since late 2022. This observation resulted in the surprising finding that the C-band (5 GHz) flux density had increased by a factor of 7 to 37.4 mJy. We immediately triggered additional DDT requests to the VLBA, EVN, VLA, AMI, e-MERLIN, and the SMA from April 2023 up to the time of this paper, on timescales ranging from every few days to monthly. As of May 2024, the source is still being monitored regularly by the VLBA, EVN, and e-MERLIN. In this initial publication, we present primarily the VLBA and EVN observations of 1ES 1927+654 to date, as well as the observations by AMI, one of the several VLA observations obtained in May 2023, and mm-band measurements by the SMA in July 2023 and June 2024.

2.2. VLBA Calibration and Imaging

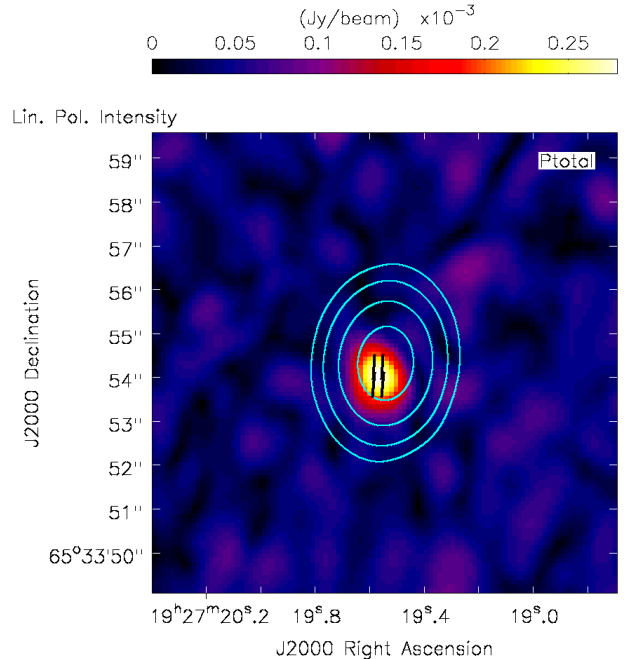


Figure 1. Total polarized intensity map at 5.5 GHz for the VLA observation of 2023-05-21. Color scale gives the flux density in mJy beam^{-1} . Contours overlaid in cyan correspond to the total (Stokes I) intensity, with levels at 10, 50, 250 and 1000 times the base value $2.5 \times 10^{-5} \text{ Jy beam}^{-1}$ which is approximately the total intensity image RMS. The vectors shown in black correspond to the measured linear polarization EVPA (no rotation applied). The polarized intensity peak appears slightly offset from the total intensity peak and has a value of 0.29 mJy, corresponding to a 0.6% polarization fraction.

The VLBI observations spanning 2013 to early 2024 are summarized in Table 1, where we describe both the VLBA observations and those from the European VLBI Network (EVN), discussed in the next section. In particular we give the observation date, program name, central frequency in GHz, and the final image RMS value in mJy/beam in columns 1-5. In columns 6 and 7 we give the peak radio flux in mJy/beam and the total radio flux of the source in mJy. The restoring beam (i.e., approximately the resolution of the imaging) is given in column 8 as the semi-major and minor ellipse axis length in mas, and the orientation of the ellipse in degrees in column 9. The final column notes whether self-calibration was possible for the imaging (‘no’ indicates it was not, while ‘p’ indicates phase-only self-calibration was applied, and ‘ap’ indicates both amplitude and phase).

Table 1. VLBA and EVN Observation and Radio Properties.

Date	Segment	Band	Freq. (GHz)	RMS (mJy bm ⁻¹)	F_{peak} (mJy bm ⁻¹)	S_{tot} (mJy)	Rest. Beam ($\alpha \times \delta$; mas)	Beam Angle (deg)	Self-calibration
<i>–Previously Published–</i>									
2013-08-10	EG079A [†]	L	1.48	0.25	18.9	...	28.2×11.7
2014-03-25	EG079B [†]	C	4.99	0.03	4.1	3.6*	2.47×1.18
2018-12-04	RSY07 [†]	C	4.99	0.04	8.4	0.7*	6.01×4.95
<i>–New Observations–</i>									
2020-01-17	BY 149	S	2.28	0.15	1.78	3.99	6.4×3.3	0.95	no
		X	8.43	0.03	0.26	1.61	1.7×1.0	5.46	no
2021-03-15	BM 518	C	4.98	0.04	1.33	5.32	3.9×1.5	15.82	no
2022-03-05	BM 527	C	4.87	0.04	2.95	5.89	3.8×2.5	28.98	no
		X	8.37	0.03	1.20	2.38	2.2×1.2	22.59	no
2022-08-05	BY 177B	C	4.87	0.03	1.89	4.95	4.0×1.6	17.88	no
2022-08-08	BY 177C	X	8.37	0.02	1.10	1.83	1.6×0.9	−4.23	no
2023-02-10	BY 177F	X	8.37	0.03	10.57	11.92	1.7×1.0	−11.48	p
2023-02-18	BY 177E	C	4.87	0.21	6.84	8.26	4.3×2.0	13.46	p
2023-04-27	BR 256	C	4.98	0.05	36.32	37.47	3.9×1.5	−5.15	a+p
		X	8.42	0.05	47.09	48.77	2.3×0.9	−8.06	a+p
2023-05-21	BM 549A	C	4.98	0.07	48.44	49.74	3.9×1.4	−4.15	a+p
		X	8.42	0.04	39.79	40.61	2.3×0.9	−6.76	a+p
2023-05-28	BM 549B	C	4.98	0.05	53.33	55.92	4.1×1.5	−4.15	a+p
		X	8.42	0.07	45.91	47.32	2.5×1.0	−5.80	a+p
2023-06-01	BM 549C	C	4.98	0.05	67.36	67.60	3.9×1.6	−9.18	a+p
		X	8.42	0.05	50.11	51.76	2.3×0.8	−9.94	a+p
2023-06-08	BM 549D	C	4.98	0.10	69.27	73.10	4.0×1.8	20.75	a+p
		X	8.42	0.13	57.22	58.58	2.2×0.8	23.17	a+p
		K	22.22	0.11	20.69	20.91	0.9×0.4	19.07	a+p
2023-06-28	RB008 [†]	C	4.93	0.08	55.59	54.58	9.2×2.7	−85.89	a+p
2023-07-22	BM 550A	C	4.87	0.07	58.42	63.82	4.0×1.8	−22.15	a+p
		X	8.37	0.10	59.42	61.29	2.4×1.0	−25.01	a+p
		K	23.55	0.21	10.90	13.05	0.8×0.4	−31.35	no
2023-08-31	BM 550B	C	4.87	0.12	52.06	54.31	3.6×1.3	−19.58	a+p
		X	8.36	0.07	53.85	55.65	2.3×0.8	−23.72	a+p
		K	23.57	0.30	5.66	5.27	0.9×0.3	−27.93	no
2023-09-23	BM 550C	C	4.87	0.12	62.26	65.50	4.6×1.6	−15.75	a+p
		X	8.36	0.11	52.07	54.55	2.8×0.9	−17.57	a+p
		K	23.57	0.30	5.06	6.30	1.0×0.4	−22.25	no
2023-10-27	BM 550D	C	4.87	0.06	64.73	65.07	4.3×2.0	−26.28	a+p
		X	8.36	0.06	50.88	54.50	2.5×1.0	−25.48	a+p
		K	23.57	0.24	7.45	19.50	0.9×0.6	27.04	no
2023-11-09	RB009 [†]	K	22.24	0.50	9.16	10.45	0.7×0.2	9.22	no
2023-11-26	BM 550E	C	4.87	0.07	54.60	59.66	4.1×1.9	−20.92	a+p
		X	8.37	0.20	45.31	46.68	2.3×0.8	−21.00	a+p
		K	23.57	0.07	13.12	15.86	0.9×0.4	−23.83	a+p

Table 1 *continued*

Table 1 (continued)

Date	Segment	Band	Freq. (GHz)	RMS (mJy bm ⁻¹)	F_{peak} (mJy bm ⁻¹)	S_{tot} (mJy)	Rest. Beam ($\alpha \times \delta$; mas)	Beam Angle (deg)	Self-calibration
2023-12-26	BM 550F	C	4.87	0.08	64.82	69.02	4.4×1.5	−21.44	a+p
		X	8.37	0.07	48.99	51.40	2.6×0.8	−24.06	a+p
		K	23.57	0.12	9.93	14.77	0.9×0.4	−32.18	p
2024-02-09	BM 556A	C	4.87	0.06	69.64	74.36	3.0×2.0	−33.80	a+p
		X	8.37	0.05	47.42	50.44	1.8×1.1	−31.59	a+p
		K	23.57	0.11	8.15	10.53	0.7×0.5	−43.13	p
2024-03-12	EB106 [†]	K	22.24	0.16	6.16	7.09	1.0×0.7	−7.68	no
2024-04-24	BM556B	C	4.87	0.08	69.30	74.47	4.6×1.4	−0.47	a+p
		X	8.37	0.05	54.04	57.97	2.7×0.9	−6.84	a+p
		K	23.57	0.14	17.10	19.52	0.9×0.4	−11.61	p

NOTE—Previously published observations (top 3 entries) taken from Laha et al. (2022).

[†]Observed by the European VLBI Network (EVN).

*fluxes were reported as central point source (PS) flux densities.

For those observations with sufficient signal/noise ratio (SNR) per antenna for reasonable short solution intervals, we applied one or more iterations of phase-only self-calibration. In some cases the SNR was insufficient to proceed further, while in others (most C and X band observations) a single additional amplitude and phase self-calibration was applied. We verified that any self-calibration applied resulted in improved image RMS, and the values reported in Table 1 correspond to the self-calibrated image where this is the case. The degree/use of self-cal is noted in the last column of Table 1.

In the initial calibration of all VLBA observations, we utilized the National Radio Astronomy Observatory (NRAO) Astronomical Image Processing System, also known as AIPS (van Moorsel et al. 1996). Specifically, we used the new primary development version of AIPS, release 31DEC23. Each frequency dataset was calibrated independently by pairing the target source with the phase calibrator (J1933+6540). We followed standard calibration procedures using VLBAUTIL and flagged bad data when necessary. We completed the calibration process for the phase calibrator and applied the calibrations to the source using the SPLIT task. Once these standard AIPS calibration procedures were finished, we proceeded to the imaging stage. We utilized the IMAGR task in AIPS to create images of both the calibrators and sources.

We utilized the NRAO Common Astronomical Software Applications (CASA; CASA Team et al. 2022)¹ to analyze images from our VLBA observations. To determine the integrated flux densities for sources, we used the two-dimensional fitting application through the VIEWER command in CASA. In Table 1, we listed the flux density values for all of our observations, along with all the radio properties of the final images.

2.3. EVN Calibration and Imaging

The three EVN epochs performed between 2023 and 2024 are summarized in Table 1. Phase-referencing was performed, adopting the same calibrator as for the VLBA observations. Data were calibrated in CASA, through the rPICARD pipeline (Janssen, M. et al. 2019). The calibrated visibilities were then imaged with DIFMAP (Shepherd 1997), following a standard phase and amplitude self-calibration procedure. Finally, integrated flux densities were extracted via a two-dimensional Gaussian fitting in CASA.

2.4. Very Large Array C-band Observations

In the high-cadence VLA observing program 23A-407, our source was observed 11 times between May 20 and June 1. Here we present the observations of 21 May 2023 which were contemporaneous with a VLBA observation, to put limits on the large-scale radio flux which may contaminate lower-resolution observation (such as with AMI), and to measure the degree of polarization in the radio, if any. A full presentation of the remaining VLA observations will be made in a forthcoming paper.

¹ <https://casa.nrao.edu>

For the 21 May 2023 observations the array was in B configuration and we used a standard 8-bit C-band continuum observing setup with 2048 MHz bandwidth. Radio frequency interference (RFI) losses resulted in a reduction of bandwidth by an estimated 15–20% on most baselines and the complete loss of spectral window 10. 3C 48 served as the primary bandpass and flux calibrator, as well as the polarization calibrator for the cross-hand delay and polarization angle, using values from 2019 available from the NRAO website (see e.g. Perley & Butler 2017). The unpolarized source J2355+4950 was used to determine instrumental polarization (leakage/D-terms), and J1927+6117 was used as a secondary gain calibrator. All calibration, imaging, and analysis was carried out with the CASA package. We used a modified version of the CASA pipeline (6.5.4.9) for the initial calibration and then determined the polarization calibration tables by hand after additional flagging of both source and calibrators for RFI. In the initial pipeline run we ran the `hifv_sypower` task with `apply=True` to counteract the effects of gain compression due to strong RFI. The CASA task `tclean` was used in interactive mode for imaging deconvolution using standard wide-band continuum parameters (mtmfs deconvolver with `nterms=2`, natural weighting). Two rounds of self-calibration were applied after initial imaging of Stokes’ I only, one phase-only followed by a cumulative amplitude+phase table. The final full-Stokes (IQUV) imaging used natural weighting with a pixel scale of $0''.1$. The resulting images have a restoring beam of $1''.6 \times 1''.2$ oriented at -4.25° . The Stokes’ I, Q, U, and V images have RMS values of 2.5, 2.1, 2.4, and 2.2×10^{-5} Jy beam $^{-1}$, respectively.

The resulting total intensity map of 1ES 1927+654 shows an unresolved point source of 53 mJy (reference frequency 5.5 GHz) with very low to zero polarization. The flux density is consistent with the VLBA flux density measurement of 49 mJy at 4.98 GHz on the same date given typical uncertainties on the absolute flux density scale of ~ 5 –10%. The linear polarization intensity map formed from the Stokes Q and U images is shown in Figure 1 and shows a point source with peak flux density 0.29 mJy, which is approximately 7 times the (polarized intensity) image RMS. However, similar low-level peaks which are clearly noise can be seen in several locations in the image, with peak levels up to ~ 0.1 mJy. The peak of polarized intensity is also not perfectly aligned with the peak in the Stokes’ I image. Thus some caution is warranted and we interpret this as an upper limit of 0.6% on the linear polarization fraction at C-band. The Stokes V image does not show any signs of an excess and

based on the V-band RMS we report an upper limit of 0.2% on the circular polarization.

2.5. Arcminute Microkelvin Imager (AMI) observations at 15.5 GHz

1ES 1927+654 was observed on many occasions between 2023 Jun 07 and 2024 April 02 with the Large Array of Arcminute MicroKelvin Imager (AMI; Zwart et al. 2008; Hickish et al. 2018). AMI consists of eight 12.8-m antennas sited at the Mullard Radio Astronomy Observatory near Cambridge, UK. The AMI receivers cover the band from 13 to 18 GHz, and are of a single linear polarisation, Stokes I+Q. We report here 58 observations taken over the above timeframe with a mean spacing of ~ 5.3 days. Analysis was done using custom software, `REDUCE_DC` (Perrott et al. 2013). Each observation consisted of multiple 10-min scans of 1ES 1927+654, interleaved with short (~ 2 -min) observations of a nearby compact source, which were used for phase calibration. The flux density scale was set using nearby observations of 3C286, which were usually made daily. The number of antennas available varied between observations, due to technical issues, and usually longer observations were made when there were fewer working antennas available. The day-to-day flux density uncertainty is estimated at $\sim 5\%$.

2.6. e-MERLIN

Regular observations from e-MERLIN cycle 16 program CY16025 were obtained as “filler” scans at C-band inserted into other accepted programs using that frequency. Partial results from this program, namely data from September to November 2023 so far have been made available as fully calibrated uvfits files. With only modest “snapshot” depth observations the UV coverage is not always sufficient for reliable imaging deconvolution, so we have opted for a non-imaging analysis method to obtain the source flux in the e-MERLIN observations. In particular, we use the CASA task `uvmodel` to fit a simple point-source model to the visibilities, adjusting the starting values to ensure stability and convergence. The model column of the MS (measurement set) file is then populated according to the fit results and we apply standard self-calibration cycles with decreasing solution intervals to then improve the applied calibration, re-running the model fit at each step. We conducted several rounds of phase-only (non-cumulative) self-calibration followed by a single round of amplitude and phase calibration. In the middle panel of Figure 2, we show the preliminary results from this program, as 3 data points corresponding to roughly weekly averages.

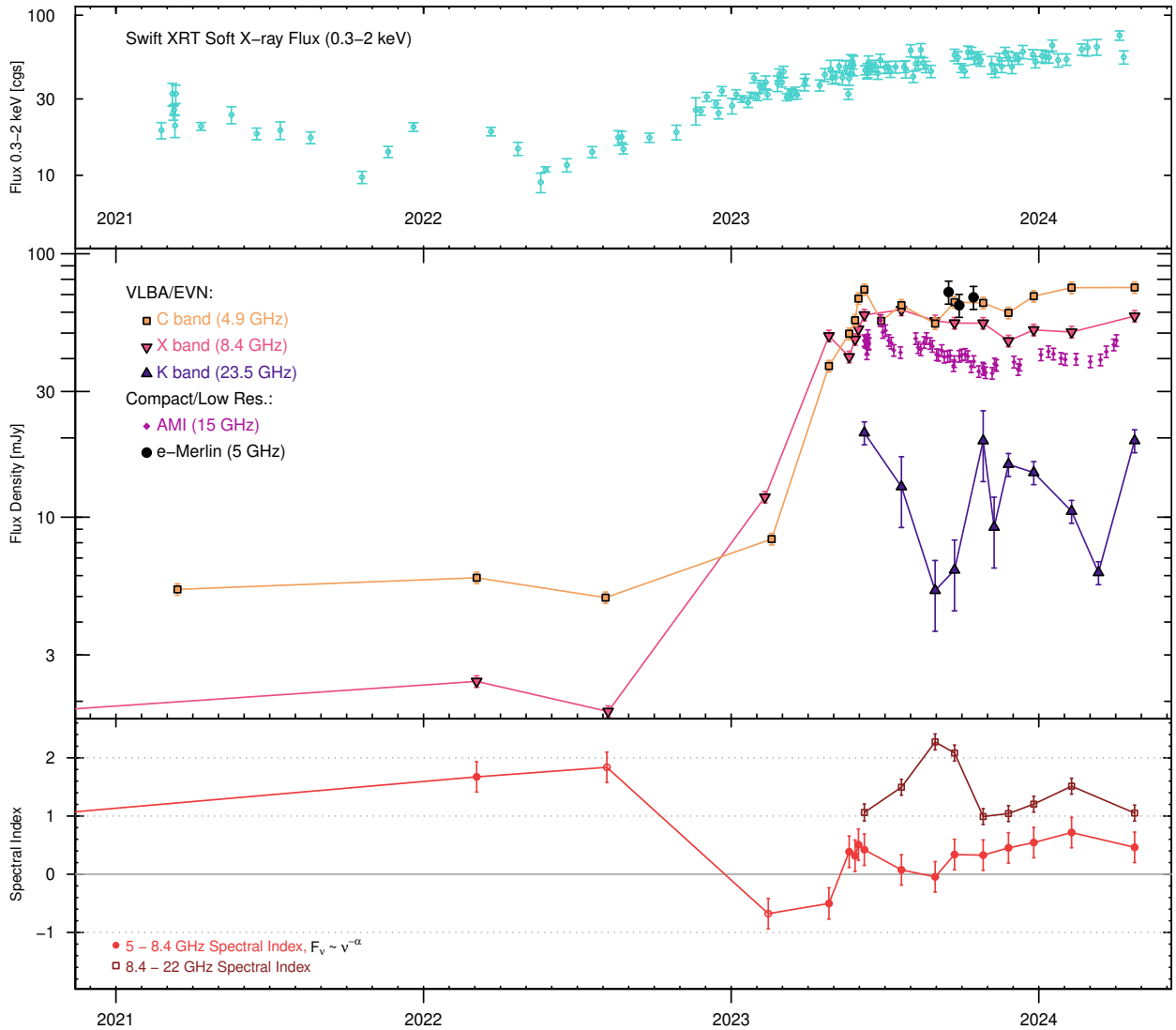


Figure 2. The soft X-ray and radio lightcurves of 1ES 1927+654 since 2021. The top panel shows the 0.3–2 keV flux (log scale) observed by the *Swift*/XRT (further details in Laha et al. 2024); central panel shows the total (log scale) VLBA/EVN flux in bands C, X, and K (5, 8.4, and 22.2/23.5 GHz, respectively) along with fluxes from lower-resolution AMI and e-MERLIN observations at 15.5 and 5 GHz respectively. The lower panel shows the evolution of the radio spectral index between 5 and 8.4 GHz (light red) and 8.4 and 22 GHz (dark red); open circles denote two epochs of near-simultaneous observations for the lower band index. While the X-rays have shown considerable variability during the years since the late 2017 CL event, the radio remained quiescent in all bands until exhibiting an exponential rise over a few months in early 2023. The radio evolution since has shown only mild variability at or slightly below the peak radio flux density reached in June 2023, with the exception of K-band.

2.7. Submillimeter Array (SMA)

The source 1ES 1927+654 was observed twice by the SMA in Hawaii, on 31 July 2023 and 11 June 2024 (hereafter epoch 1 and 2). In both observations there were six SMA antennas operating in similar compact configurations with baselines up to ~ 80 m. In epoch 1 the target was observed in a single frequency band using two orthogonally polarized double sideband receiver sets, each processing 12 GHz of bandwidth per sideband (provid-

ing a total of 48 GHz of processed bandwidth) centered at a frequency of 225.5 GHz ($\lambda \sim 1.35$ mm). In epoch 2 the observation included simultaneous dual band observations, each with a single polarization (providing 24 GHz of processed bandwidth each), one again centered at 225.5 GHz and the other at 347 GHz ($\lambda \sim 870$ μm). The weather was very good in both observations, with the water vapor column ranging between 1.5 and 2 mm pwv. Observations of 1ES 1927+654 were in-

terleaved with observations of nearby gain calibration sources, J1806+698 and J1927+739, with the absolute flux scale calibrated primarily against the continuum of MWC349A, with added checking in epoch 1 using Ceres and Callisto. Standard reduction using the SMA MIR calibration suite was performed for both epoch 1 and 2.² The data for epoch 2 were also processed using the COMPASS pipeline reduction package which provides several improved and automated steps for data flagging and quality control (Keating, private communication). The total usable on-source integration time was 7.13 hours and 6.97 hours for epochs 1 and 2, respectively. The synthesized spatial resolution at 225.5 GHz was similar for both epochs, $\sim 3.'' \times 3.0''$, while the higher frequency band in epoch 2 at 347 GHz achieved a resolution of $2.2'' \times 1.9''$. For epoch 1 (225.5 GHz), the flux density was found to be 5.49 ± 0.29 mJy, determined from a vector average of the calibrated visibility data, and confirmed using imaging using the AIPS task IMAGR. For epoch 2, the flux density at 225.5 GHz was measured to be 5.73 ± 0.35 mJy (consistent with epoch 1), and at 347 GHz the flux density was 4.57 ± 1.27 mJy using the COMPASS pipeline reduction and imaging path.

3. RESULTS AND DISCUSSION

3.1. Radio Lightcurve and SED evolution

In Figure 2 we show the main result for 1ES 1927+654, which is a ~ 40 – and 60-fold increase at 5 and 8.4 GHz in the core radio flux density over a very short time period from January to June 2023. The upper panel shows the 0.3–2 keV soft X-ray flux as seen by *Swift*/XRT for comparison (see Laha et al. (2024) for further details). The central panel shows the total radio flux in the VLBA observations at 5.4, 8.4, and 22.2/23.5 GHz (C, X, and K-band) as well as fluxes from lower-resolution instruments e-MERLIN (5 GHz) and AMI (15.5 GHz). The 5–8.4 GHz and 8.4–23 GHz spectral indices are shown in the lower panel over the same timeframe. The peak radio flux was likely reached between the 8 June and 22 July epochs of VLBA monitoring, in agreement with the peak in the AMI lightcurve on 27 June. The 5.4–8.4 GHz spectral index became notably “flat” ($\alpha < 0.5$ for $\nu^{-\alpha}$) during the fast rise in early 2023, and has remained so in nearly all epochs in the year following.

The near-weekly cadence of VLBA observations in May–June 2023 fortunately caught the source during the exponential rise phase. A fit to the six C-band observations from 18 February to 8 June 2023 with an exponential function gives a characteristic timescale of \sim

44 days, with an equivalent light-crossing size limit of about 0.04 pc (assuming no significant beaming). This is just below the resolution of our K-band VLBA imaging which has a synthesized beam on the order of 0.4–0.8 mas or 0.15–0.30 pc. In the nearly 1 year since the radio outburst began, the source has maintained near-peak radio luminosity with only low-level variability from 5–15.5 GHz. The 22.2–23.6 GHz K-band flux shows a somewhat higher degree of variability, though this may be in part due to decoherence losses as self-calibration was not always possible in this band, and the effects of a weaker delay calibration source in the BM550A-D observations (we adopt a larger error bar of 30% vs. a standard 10% for the non-self-calibrated epochs in Figure 2). The average 5.4 GHz flux density of 65 mJy since the peak in 2023 June corresponds to a radio power of $\nu L_{\nu, R} = 2.6 \times 10^{39}$ erg s⁻¹.

The VLBI-resolution radio spectral energy distribution from 2020 January to 2024 April ($\log F_{\nu}$ vs $\log \nu$) is shown in Figure 3, where we plot the total flux density. The spectrum is notably curved with a peak at or just below 5 GHz with an appearance similar to Gigahertz-peaked spectrum (GPS) AGN sources, as further discussed below. We also include in this figure SMA observations from June 2024, at 225 and 345 GHz (the 2023 July observation at 225 GHz only resulted in an almost identical flux value to that of 2024 and is not shown). Both the sub-mm band SMA 225–345 GHz spectral index ($\alpha = 0.1 \pm 0.6$) and that between 23.6–225 GHz ($\alpha = 0.58 \pm 0.28$) suggests spectral hardening compared to the much steeper spectrum at the same epoch measured between 8.4 and 23.6 GHz ($\alpha = 1.05 \pm 0.26$). While the SMA observations are much lower resolution and could include a contribution from arcsecond-scale emission (i.e. cold dust), the nearly flat sub-mm spectrum is consistent with the observations and expectations of synchrotron emission from a compact corona (Raginski & Laor 2016, e.g.) rather than the Rayleigh-Jeans tail of a cold dust component. Additional higher-frequency observations should help clarify the degree of jet contribution to the SMA band and better constrain a possible turnover above 300 GHz.

3.2. Extended Source Structure and Proper Motion

VLBA imaging of 1ES 1927+654 has previously shown a low-level resolved component on \sim few pc scales with a typical flux of no more than a few mJy. As previously presented in Laha et al. (2022), the C-band (5.4 GHz) VLBA image of the source taken in 2021 March shows a central peak of approximately 2 mJy beam⁻¹ while the total flux is 5.5 ± 0.5 mJy (indicating a resolved component). Fitting of the visibilities with a modified ver-

² <https://lweb.cfa.harvard.edu/rtdc/SMAdata/process/mir/>

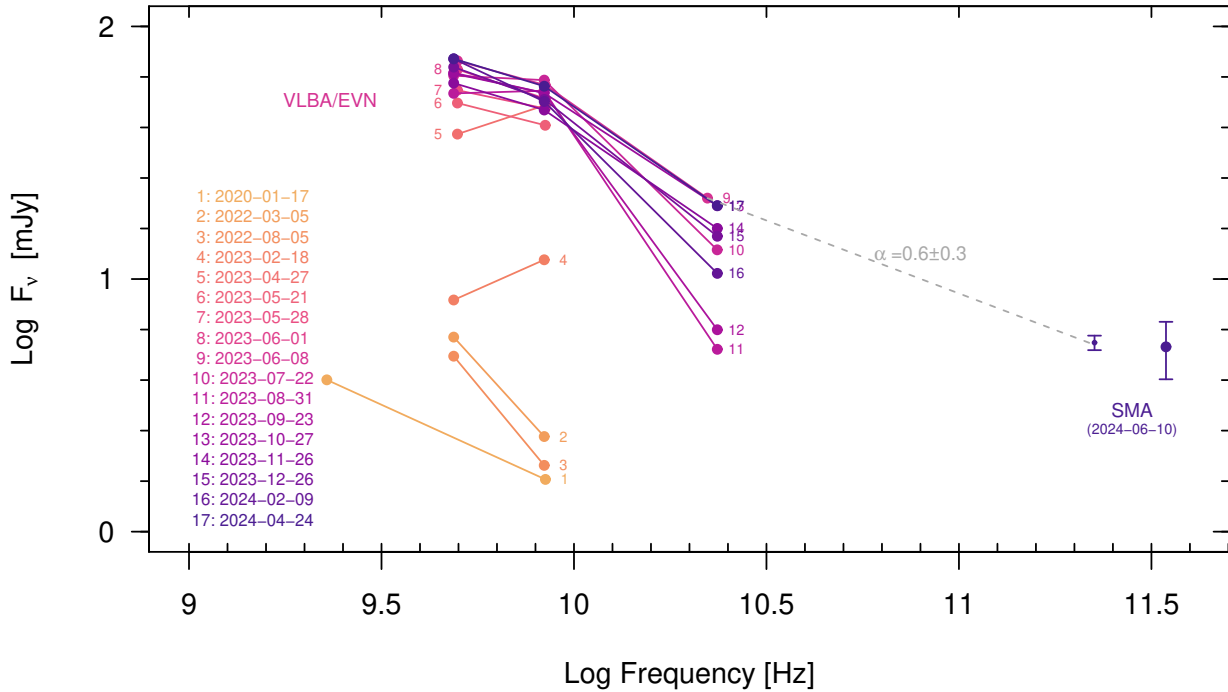


Figure 3. Plots of the radio spectral energy distribution (VLBI and SMA only), from 2020 January through 2024 April. As shown, the source exhibited a flat/hard spectrum during the initial rise in early 2023, but since then shows a fairly consistent GHz-peaked spectrum. The peak of the spectrum appears to be at or just below 5 GHz. The SMA observations shown were taken on 10 June 2024 at 225 and 345 GHz and suggest a flat spectrum ($\alpha = 0.1 \pm 0.6$) in the sub-mm band, possibly consistent with a coronal origin. The 225 GHz flux in June 2024 was almost exactly the same as the value obtained in July 2023 at the same frequency.

sion of DIFMAP (Roychowdhury 2023; Shepherd et al. 1994) showed that the extended flux was consistent with a disk-like component of uniform surface brightness (total flux ~ 4 mJy) and a size of $3.5 \times 4.5 \text{ mas}^2$ ($1.3 \times 1.7 \text{ pc}^2$). Similar results for the peak and extended component were obtained for the March and August 2022 observations, with some hints of a reduction in the disk size (by $\sim 20\%$) in the latter epoch (Ghosh et al. 2023). Surprisingly, the extended component was not detected at all (size $< 0.1 \text{ pc}$, flux $< 0.1 \text{ mJy}$) at C-band by 27 April 2023, when the unresolved core had begun to rise. It is possible that this emission arose from the slowly-expanding result of a previous outburst which became optically thin and went below the level of detection by early 2023; unfortunately we lack multi-band observations from that time for a more clear spectral analysis.

While a detailed investigation of the source structure through visibility-fitting of all VLBA epochs is deferred to a future publication, we show in Figure 4 core-subtracted K-band VLBA images from 8 June 2023 at

22.2 GHz (epoch BM549D) and 9 February and 24 April 2024 at 23.6 GHz (epochs BM556A/B). The February 2024 observation is deeper due to combining the allotted time of two observations from a nominally monthly monitoring program (7 hr vs 3.5 hr scheduling block). These images were produced after one round of phase-only self-calibration. In each case we used a very small clean box region of only a few pixel extent over the core region and very slow clean cycles (`cycleniter=1-40`) to produce a core-only model in the measurement set, stopping at the same residual flux level (approx. $0.19 \text{ mJy beam}^{-1}$) in the central core region for the Feb and April 2024 epochs. (Since no residual emission at all was apparent in June 2023, we continued to the level of the image RMS). The core emission in all cases was then removed using the CASA task `uvsub`, before re-imaging the resulting measurement set.

The residual emission, of which there is no sign in June 2023, has a total flux of 3.7 mJy in both the later epochs, compared to the total integrated flux including

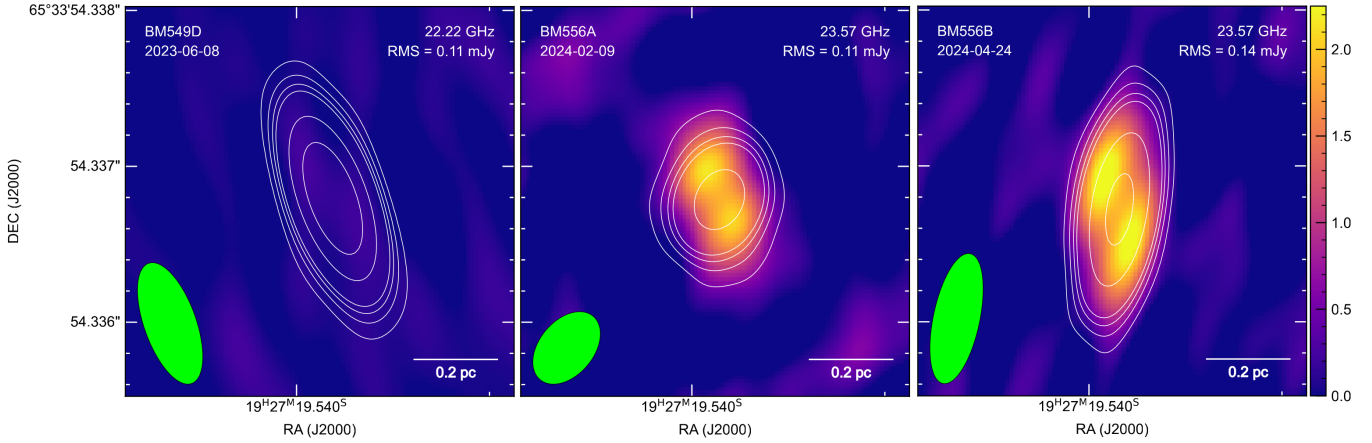


Figure 4. Core-subtracted K-band VLBA images of 1ES 1927+654 from 8 June 2023 (left), 9 February 2024 (center) and 24 April 2024 (right) — the latter two are the two most recent epochs in Figure 2. The contours correspond to the non-core-subtracted intensity and are drawn at 5, 10, 15, 20 and 50 times the non-core-subtracted image RMS (given at upper right in each panel). The longer February 2024 observation resulted in better UV coverage and a less elongated synthesized beam than the other two observations (green oval at lower left in each panel). The extended structure apparent in Feb and April 2204 is entirely absent at the time of the initial radio outburst in June 2023, and has a total flux of 3.7 mJy in both epochs where it is detected.

the core of 10.5 mJy in February and 19.5 mJy in April 2024. After subtraction, the two peaks apparent in the residual images are orientated at the same position angle of $\sim 293^\circ$. In February the separation of peaks is 0.35 mas or 0.13 pc, while in April the separation is measured to be somewhat larger, at 0.45 mas or 0.16 pc. Naively adopting these measurements corresponds to a jet advance speed $0.3c$, which is similar to the value implied from the current extent assuming the outflow began with the onset of the radio flare in February 2023 ($0.2\text{--}0.25c$). This also matches the outflow speeds inferred from the 1 keV emission line seen during the super-Eddington state of 2020–2021 – a time when radio observations were unfortunately lacking (Masterson et al. 2022).

A full kinematic analysis requires continued monitoring and more accurate positions through UV-plane fitting with e.g. DIFMAP which is beyond the scope of the current publication given the few deep epochs available.³ If the extended resolved features represent a jet-driven outflow, continued observations of the source should more clearly resolve these components with time. In at least one other CL-AGN, Mkn 590, a pc-scale jet-like extension has been observed years after the event (Yang et al. 2021), however that source did not display

a dramatic radio flare and the total radio power is considerably lower.

3.3. Source of the radio emission

Radio emission in radio-quiet AGN can arise from a number of sources including star formation and shocks from AGN-driven winds, small-scale jets, and/or the same compact corona that gives rise to X-ray emission (see e.g. Panessa et al. 2019, for a recent review). In 1ES 1927+654, the first two origins can be ruled out easily based on both variability and physical scale. Indeed, comparison of low-resolution VLA and AMI observations taken at the same time as our VLBA observations shows no significant difference in total flux as might be expected if radio emission on larger scales (which would be resolved out by the VLBA) were significant. A strictly coronal origin for the GHz band compact emission is also precluded based on the requirements inferred from the X-ray observations (Laha et al. 2024), i.e. the very small size ($\sim 10 r_g$) and high magnetic field strength (on the order of $10^4\text{--}10^5$ G). Besides very strong synchrotron self-absorption (SSA) which would be expected in such a source, there will be no significant synchrotron emission below the cyclotron frequency of $\sim (30\text{ GHz})(B/1e4\text{ G})$.

A small-scale synchrotron jet/outflow thus appears most consistent with the radio emission, even before the recent radio outburst. In this case the unresolved radio emission we observe arises on much larger scales than the X-ray emitting corona. Taking a flux of 45 mJy at 15 GHz and radio spectral index $\alpha = 1$ as typical values since the flare began, and assuming a source size of 0.05 pc, we use the minimum-energy condition (equipar-

³ The EVN K-band observations, though reaching comparable theoretical sensitivity to the VLBA due to long total observing times, lack the short-timescale signal/noise required for self-calibration and the requisite medium-scale spacings in UV coverage to detect the extended components. However 1ES 1927+654 is approved for continued VLBA monitoring with deeper K-band observations through 2025.

tion) to derive a magnetic field for emitting region of $B=0.3$ G. Assuming a mildly relativistic jet of speed $\beta = v/c = 0.3$, this corresponds to a minimum kinetic power on the order of 10^{43} erg s $^{-1}$.

For a synchrotron origin, the lack of polarization for 1ES 1927+654 in the 5 GHz VLA observation does not necessarily cause a problem, since internal Faraday depolarization is expected at the self-absorption frequency unless the plasma is dominated by highly relativistic electrons, with a lower-bound cutoff of $\gamma_{\min} \sim 10^2$ (Jones & O’Dell 1977), as is likely the case in more powerful jets (i.e. blazars). Indeed, high rotation measures and low observed radio polarization are typical of GPS sources (O’Dea 1998).

While a full exploration of the X-ray and other multi-wavelength observations of this source are given in the companion publication by Laha et al. (2024), we can make some brief comments here. First, that the X-ray to radio luminosity (10^4) is far too high for both to arise from nonthermal processes in a very compact jet (i.e. inverse Compton emission) as is likely occurring in e.g., Compact Symmetric Objects (CSO, Sobolewska et al. 2023). Using the equipartition value of the magnetic field and assuming a ‘light’ jet (electron-positron), and sub-relativistic speed of $0.3c$, we estimate a minimum total kinetic power for the jet of 10^{43} erg s $^{-1}$, which is comparable to the observed power radiated in soft X-rays as of mid-2024. The onset of the soft X-ray rise just before the radio, as well as the spectral shape in the soft X-rays, could be consistent with shocked gas being driven by the newly launched radio jets, as an alternative to a coronal origin. In either case, assuming the X-ray and radio emission are related, the delay in the radio emission could be due to the presence of screening material (hot gas) on small scales. Alternatively, the jet/outflow may be either too compact or simply inefficient at particle acceleration in the initial phase.

3.4. Comparison with young/short-lived jet classes

As noted, the current spectrum of the source bears some resemblance to GPS sources, which are understood to be relatively recently-formed radio jets, typically of age less than 1000 years and size less than 1 kpc (e.g. O’Dea & Saikia 2021). In these sources the compact radio source arises from synchrotron emission which suffers either SSA or free-free absorption. The advance speeds of these jets are typically low, on the order of 0.1 – $0.2c$ or less. A related class of sources are known as compact symmetric objects or CSO, which are double-lobed radio sources off less than 1 kpc in extent (Readhead et al. 1994, 1996). Unlike GPS sources, the class is primarily a morphological one and requires high-resolution radio

imaging for identification. They are often similarly identified as young radio sources $\lesssim 1000$ yr in age and have relatively slow rates of growth in size, of $\sim 0.3c$ on average (Taylor et al. 2000; An & Baan 2012). In terms of their radio spectra, most CSO sources (e.g. 82% in the study of Tremblay et al. 2016) exhibit a GPS-like spectrum, and can be core or lobe-dominated (type 1 or 2, respectively). Very recent work on the kinematics of a carefully selected sample of mostly CSO-2 suggests that they should be considered a distinct class of ‘short-lived’ jets rather than simply young versions of more classical powerful radio-loud AGN (Kiehlmann et al. 2023). This fits well with the idea that CSO-type jet activity is powered by a “single fueling event”, e.g. the capture of a single star by the central black hole (Readhead et al. 1994; An & Baan 2012; Kiehlmann et al. 2024).

Although direct evidence of newly formed radio jets in AGN are rare, it is not unprecedented. A recent study comparing the VLA All-Sky Survey (VLASS) epoch 1 observations (2017–2019) to the earlier FIRST (Faint Images of the Radio Sky at Twenty cm; 1993–2011) survey discovered 14 new radio-loud sources which have turned on sometime in the last ~ 20 yr, and these also have peaked radio spectra resembling GPS sources (Nyland et al. 2020). The radio emission was roughly constant on few-month timescales on VLA follow-up, and the typically tens-of-GHz frequencies of the radio spectral peaks appear consistent with the expected size–peak frequency relation of young jets (O’Dea 1998; Jeyakumar 2016).

While there is clear similarity between the case of 1ES 1927+654 and known young/short-lived jets, the radio powers of classical CSO and GPS sources are generally much higher than 1ES 1927+654, by a factor of >100 (O’Dea 1998; O’Dea & Saikia 2021). Even for the recently discovered VLASS sources, which extend down to lower radio power ($\log L_{3\text{ GHz}} = 40.5$) than classical GPS samples, the lowest is still an order of magnitude more powerful in the radio than 1ES 1927+654. However this may simply reflect the “down-sized” nature of 1ES 1927+654 which likely hosts a central black hole of only $\sim 10^6 M_{\odot}$ (Li et al. 2022). While there are some indications that GPS sources have somewhat smaller black hole masses on average than their classical radio-loud QSO cousins (e.g. Gu et al. 2009; Wu 2009), typical values are on the order of $\log M_{\text{BH}} \sim 8$, or 100x that of 1ES 1927+654. It is plausible that the lack of lower-power CSO sources in our current samples may simply be a selection effect. Indeed, although focusing on the far more prevalent non-CSO jet classes, the LOFAR Two-Metre Sky Survey found that the morphological class of edge-brightened (FR II) type jets, for decades thought to

occur only at relatively high luminosities, actually extend down to luminosities 3 orders of magnitude below the traditional Fanaroff & Riley division (Mingo et al. 2019). As CSO sources appear to be relatively rare (6-8%) in radio-selected AGN samples, and only recently have moderately sized complete samples been compiled (e.g. 79 sources in Kiehlmann et al. 2024), deeper surveys may well uncover more objects like 1ES 1927+654.

3.5. Comparison to late-time radio flares in TDEs

One observation that bears further exploration is the initial exponential rise in radio flux for 1ES 1927+654, which is in contrast with the prediction of a much slower $P \propto t^{2/5}$ behavior predicted for the turn-on of GPS sources (An & Baan 2012). In addition, it is unclear what, if any, relation the current radio outburst has to the TDE-like changing-look event which occurred in early 2018 or the super-Eddington accretion phase which followed over a year later and lasted into mid-2020. Tidal disruption events, in which a star passing too near a non-active central black hole is tidally disrupted, producing a characteristic flare in the optical, UV and (frequently) X-rays, are seen to produce prompt radio emission (within ~ 100 days) in only about 20-30% of cases. The radio is typically attributed to synchrotron emission from the interaction of outflows with circum-nuclear material, as well as shocks formed in debris-stream collisions or, more rarely, relativistic jets (see Alexander et al. 2020, for a recent review).

Interestingly, very recent work shows that late-time radio activity actually occurs in at least 50% of TDE with initial non- or low-level detections, with onset times ranging from a few hundred to >1000 days (Cendes et al. 2023, and references therein), and frequently with very fast rise timescales, e.g. faster than $F_\nu \propto t^5$ in AT2018hyz (Cendes et al. 2022). The latter case may be consistent with an off-axis relativistic jet, where the radio emission is initially ‘beamed away’ before the jet decelerates enough to become visible (Sfaradi et al. 2023, but see also Cendes et al. 2022). However misaligned jets cannot explain the majority of cases, most directly because of the high rate of on-axis jetted TDE implied, which is not observed, and also because a decelerating jet scenario typically predicts a radio peak on the order of 100 days after onset, far less than the observed values of $\gtrsim 700$ days (Matsumoto & Piran 2023; Cendes et al. 2023; Beniamini et al. 2023). The origin of the probable outflows responsible for late-time radio emission in TDE is still under discussion, however Matsumoto & Piran (2024) are able to explain delays up to those observed ($\sim 10^3$ days) as a natural consequence of non-relativistic to very mildly relativistic outflows ($\beta < 0.15$) and the ef-

fects of a flattening density profile of the circum-nuclear material.

TDE in existing AGN are theoretically expected (e.g. Chan et al. 2019) but are challenging to convincingly detect due to competition from normal AGN flares (e.g. Auchettl et al. 2018). Interestingly, some recent theoretical work has suggested that TDE in existing AGN may precipitate changing-look events (Wang et al. 2024). The case of 1ES 1927+654 does show some similarities to TDE with late-time radio emission. The timescale is only slightly longer than the most delayed onset in TDE seen so far (at ~ 1800 days), though one of the key conclusions of the recent discovery of late-time emission is that further long-term follow-up, possibly on decade timescales, is needed to fully characterize the phenomenon (Cendes et al. 2023). Alexander et al. (2020) also note that a significant outflow may only be launched after (and if) the accretion onto the BH reaches a super-Eddington phase. For 1ES 1927+654 the time delay of the radio onset from that period in 2020 is ~ 1000 days.

If our initial estimate of an outflow of speed $\sim 0.3c$ stands, then the outflow in 1ES 1927+654 is in an interesting middle regime between the sub-relativistic outflows inferred in the sample of late-time TDE radio sources and the relativistic jets seen in small fractions of both AGN and TDE. The radio luminosity of 1ES 1927+654 is comparable to or slightly above the upper end of what is seen for non-relativistic TDE outflows (typically $< 10^{39}$ erg/s) but well below that of most radio-loud AGN or e.g., the famous jetted TDE Swift J1644+57 (Berger et al. 2012). The BH mass of 1ES 1927+654 may explain some of the similarity in energy scale, as the BH masses for TDE tend to be substantially smaller than in AGN on average (e.g., $5 \times 10^5 - 10^7 M_\odot$ in the sample of Ryu et al. 2020) reflecting the population of quiescent BH and the fact that disruption events around BH larger than $\sim 10^8 M_\odot$ do not produce observable radiation. However, a down-sized black hole does not mean that highly relativistic jets cannot form, as clearly demonstrated by the recent discoveries of relativistic, gamma-ray emitting jets in narrow-line Seyfert galaxies (e.g. Foschini et al. 2015) as well as low-power but highly collimated/fast FR II jets, mentioned previously (Mingo et al. 2019). It seems likely that the difference comes down to the nature of jet-launching itself, and further study of sources like 1ES 1927+654 will be key to advancing our understanding.

4. CONCLUSIONS

A little over 5 years after it became one of extremely few AGN with a directly-observed changing-look event

(Trakhtenbrot et al. 2019), 1ES 1927+654 has recently exhibited a significant radio flare consistent with a newly-launched radio-emitting outflow, approximately 1800 days after the initial CL event. A fortuitously timed weekly VLBA monitoring program in May to June 2023 caught the exponential rise and peak of the radio onset, which reached a level of 40 and 60 times previous radio core luminosities at 5 and 8.4 GHz, respectively. The source has maintained a relatively steady radio emission with a spectrum reminiscent of gigahertz-peaked sources, for over 1 year without obvious signs of fading or further increase. The soft X-ray emission, which began rising a few months prior to the flare, may arise from shock-heated gas impacted by the jet; in this scenario the radio jet was at first screened by hot gas before breaking through, consistent with the later fast exponential rise time. Our most recent high-resolution VLBA imaging at 23.6 GHz shows bipolar radio extensions of similar brightness on 0.1-0.15pc scales, with a tentative expansion speed of 0.2-0.3c. The source therefore bears some similarity to compact symmetric objects (CSO) at 100x lower luminosity than typical for that class. The outflow characteristics also bear some resemblance to those of tidal disruption events with late-time radio emission, though as noted in previous works, the X-ray properties of this source are considerably different from a TDE, likely due to the presence of a pre-existing accretion disk. Continued follow-up with high-resolution and multi-frequency radio observations will allow us to further constrain the kinematics and energetics of the outflow in this ever-changing and unique AGN.

Facilities: Very Large Array (VLA); Very Long Baseline Array (VLBA); European VLBI Network (EVN); Arcminute Microkelvin Imager (AMI); enhanced Multi Element Remotely Linked Interferometer Network (e-MERLIN); Submillimeter Array (SMA); Swift X-ray Observatory

1 The National Radio Astronomy Observatory is a fa-
 2 cility of the National Science Foundation operated un-
 3 der cooperative agreement by Associated Universities,
 4 Inc. This work made use of the Swinburne University
 5 of Technology software correlator, developed as part of
 6 the Australian Major National Research Facilities Pro-
 7 gramme and operated under licence.

8 e-MERLIN is a National Facility operated by the Uni-
 9 versity of Manchester at Jodrell Bank Observatory on
 10 behalf of STFC, part of UK Research and Innovation.

11 We thank the Mullard Radio Astronomy Observatory
 12 staff for the AMI observations.

13 We acknowledge Phil Cigan and the MultiColorFits
 14 package which was used to create the image figures
 15 (Cigan 2019).

16 MN is supported by the European Research Coun-
 17 cil (ERC) under the European Union’s Horizon 2020
 18 research and innovation programme (grant agree-
 19 ment No. 948381) and by UK Space Agency Grant
 20 No. ST/Y000692/1.

21 The Submillimeter Array is a joint project between
 22 the Smithsonian Astrophysical Observatory and the
 23 Academia Sinica Institute of Astronomy and Astro-
 24 physics and is funded by the Smithsonian Institution
 25 and the Academia Sinica. Maunakea, the location of
 26 the SMA, is a culturally important site for the indige-
 nous Hawaiian people; we are privileged to study the

REFERENCES

- Alexander, K. D., van Velzen, S., Horesh, A., & Zauderer, B. A. 2020, *SSRv*, 216, 81, doi: [10.1007/s11214-020-00702-w](https://doi.org/10.1007/s11214-020-00702-w)
- An, T., & Baan, W. A. 2012, *ApJ*, 760, 77, doi: [10.1088/0004-637X/760/1/77](https://doi.org/10.1088/0004-637X/760/1/77)
- Antonucci, R. 1993, *ARAA*, 31, 473, doi: [10.1146/annurev.aa.31.090193.002353](https://doi.org/10.1146/annurev.aa.31.090193.002353)
- Auchettl, K., Ramirez-Ruiz, E., & Guillochon, J. 2018, *ApJ*, 852, 37, doi: [10.3847/1538-4357/aa9b7c](https://doi.org/10.3847/1538-4357/aa9b7c)
- Beniamini, P., Piran, T., & Matsumoto, T. 2023, *MNRAS*, 524, 1386, doi: [10.1093/mnras/stad1950](https://doi.org/10.1093/mnras/stad1950)
- Berger, E., Zauderer, A., Pooley, G. G., et al. 2012, *ApJ*, 748, 36, doi: [10.1088/0004-637X/748/1/36](https://doi.org/10.1088/0004-637X/748/1/36)
- Bianchi, S., Maiolino, R., & Risaliti, G. 2012, *Advances in Astronomy*, 2012, 782030, doi: [10.1155/2012/782030](https://doi.org/10.1155/2012/782030)
- Boller, T., Voges, W., Denefeld, M., et al. 2003, *A&A*, 397, 557, doi: [10.1051/0004-6361:20021520](https://doi.org/10.1051/0004-6361:20021520)
- CASA Team, Bean, B., Bhatnagar, S., et al. 2022, *PASP*, 134, 114501, doi: [10.1088/1538-3873/ac9642](https://doi.org/10.1088/1538-3873/ac9642)
- Cendes, Y., Berger, E., Alexander, K. D., et al. 2022, *The Astrophysical Journal*, 938, 28, doi: [10.3847/1538-4357/ac88d0](https://doi.org/10.3847/1538-4357/ac88d0)
- . 2023, Ubiquitous Late Radio Emission from Tidal Disruption Events, arXiv. <http://arxiv.org/abs/2308.13595>
- Chan, C.-H., Piran, T., Krolik, J. H., & Saban, D. 2019, *The Astrophysical Journal*, 881, 113, doi: [10.3847/1538-4357/ab2b40](https://doi.org/10.3847/1538-4357/ab2b40)
- Cigan, P. 2019, MultiColorFits: Colorize and combine multiple fits images for visually aesthetic scientific plots, *Astrophysics Source Code Library*, record ascl:1909.002
- Foschini, L., Berton, M., Caccianiga, A., et al. 2015, *A&A*, 575, A13, doi: [10.1051/0004-6361/201424972](https://doi.org/10.1051/0004-6361/201424972)
- Ghosh, R., Laha, S., Meyer, E., et al. 2023, *ApJ*, 955, 3, doi: [10.3847/1538-4357/aced92](https://doi.org/10.3847/1538-4357/aced92)
- Gu, M. F., Pak, S., & Ho, L. C. 2009, *Astronomische Nachrichten*, 330, 253, doi: [10.1002/asna.200811169](https://doi.org/10.1002/asna.200811169)
- Hickish, J., Razavi-Ghods, N., Perrott, Y. C., et al. 2018, *MNRAS*, 475, 5677, doi: [10.1093/mnras/sty074](https://doi.org/10.1093/mnras/sty074)
- Janssen, M., Goddi, C., van Bemmell, I. M., et al. 2019, *Astronomy & Astrophysics*, 626, A75, doi: [10.1051/0004-6361/201935181](https://doi.org/10.1051/0004-6361/201935181)
- Jeyakumar, S. 2016, *MNRAS*, 458, 3786, doi: [10.1093/mnras/stw181](https://doi.org/10.1093/mnras/stw181)
- Jones, T. W., & O'Dell, S. L. 1977, *ApJ*, 214, 522, doi: [10.1086/155278](https://doi.org/10.1086/155278)
- Kiehlmann, S., Readhead, A. C. S., O'Neill, S., et al. 2023, Compact Symmetric Objects – II Confirmation of a Distinct Population of High-Luminosity Jetted Active Galaxies, arXiv. <http://arxiv.org/abs/2303.11359>
- Kiehlmann, S., Lister, M. L., Readhead, A. C. S., et al. 2024, *The Astrophysical Journal*, 961, 240, doi: [10.3847/1538-4357/ad0c56](https://doi.org/10.3847/1538-4357/ad0c56)
- Kokubo, M., & Minezaki, T. 2020, *MNRAS*, 491, 4615, doi: [10.1093/mnras/stz3397](https://doi.org/10.1093/mnras/stz3397)
- Komossa, S., Grupe, D., Gallo, L. C., et al. 2020, *A&A*, 643, L7, doi: [10.1051/0004-6361/202039098](https://doi.org/10.1051/0004-6361/202039098)
- Laha, S., Meyer, E., Roychowdhury, A., et al. 2022, *ApJ*, 931, 5, doi: [10.3847/1538-4357/ac63aa](https://doi.org/10.3847/1538-4357/ac63aa)
- . 2024, *ApJ*, submitted, 1
- Li, R., Ho, L. C., Ricci, C., et al. 2022, *ApJ*, 933, 70, doi: [10.3847/1538-4357/ac714a](https://doi.org/10.3847/1538-4357/ac714a)
- Masterson, M., Kara, E., Ricci, C., et al. 2022, *ApJ*, 934, 35, doi: [10.3847/1538-4357/ac76c0](https://doi.org/10.3847/1538-4357/ac76c0)
- Mathur, S., Denney, K. D., Gupta, A., et al. 2018, *ApJ*, 866, 123, doi: [10.3847/1538-4357/aadd91](https://doi.org/10.3847/1538-4357/aadd91)
- Matsumoto, T., & Piran, T. 2023, *Monthly Notices of the Royal Astronomical Society*, 522, 4565, doi: [10.1093/mnras/stad1269](https://doi.org/10.1093/mnras/stad1269)
- . 2024, Late-time Radio Flares in Tidal Disruption Events, arXiv. <http://arxiv.org/abs/2404.15966>
- Mingo, B., Croston, J. H., Hardcastle, M. J., et al. 2019, *MNRAS*, 488, 2701, doi: [10.1093/mnras/stz1901](https://doi.org/10.1093/mnras/stz1901)
- Nicholls, B., Brimacombe, J., Kiyota, S., et al. 2018, *The Astronomer's Telegram*, 11391, 1
- Nyland, K., Dong, D. Z., Patil, P., et al. 2020, *ApJ*, 905, 74, doi: [10.3847/1538-4357/abc341](https://doi.org/10.3847/1538-4357/abc341)
- O'Dea, C. P. 1998, *PASP*, 110, 493, doi: [10.1086/316162](https://doi.org/10.1086/316162)
- O'Dea, C. P., & Saikia, D. J. 2021, *AAPR*, 29, 3, doi: [10.1007/s00159-021-00131-w](https://doi.org/10.1007/s00159-021-00131-w)
- Panessa, F., Baldi, R. D., Laor, A., et al. 2019, *Nature Astronomy*, 3, 387, doi: [10.1038/s41550-019-0765-4](https://doi.org/10.1038/s41550-019-0765-4)
- Perley, R. A., & Butler, B. J. 2017, *ApJS*, 230, 7, doi: [10.3847/1538-4365/aa6df9](https://doi.org/10.3847/1538-4365/aa6df9)
- Perlman, E. S., Stocke, J. T., Schachter, J. F., et al. 1996, *ApJS*, 104, 251, doi: [10.1086/192300](https://doi.org/10.1086/192300)
- Perrott, Y. C., Scaife, A. M. M., Green, D. A., et al. 2013, *MNRAS*, 429, 3330, doi: [10.1093/mnras/sts589](https://doi.org/10.1093/mnras/sts589)
- Raginski, I., & Laor, A. 2016, *MNRAS*, 459, 2082, doi: [10.1093/mnras/stw772](https://doi.org/10.1093/mnras/stw772)
- Ramos Almeida, C., & Ricci, C. 2017, *Nature Astronomy*, 1, 679, doi: [10.1038/s41550-017-0232-z](https://doi.org/10.1038/s41550-017-0232-z)
- Readhead, A. C. S., Taylor, G. B., Xu, W., et al. 1996, *ApJ*, 460, 612, doi: [10.1086/176996](https://doi.org/10.1086/176996)

- Readhead, A. C. S., Xu, W., Pearson, T. J., Wilkinson, P. N., & Polatidis, A. G. 1994, in *Compact Extragalactic Radio Sources*, ed. J. A. Zensus & K. I. Kellermann, 17
- Ricci, C., Kara, E., Loewenstein, M., et al. 2020, *ApJ*, 898, L1, doi: [10.3847/2041-8213/ab91a1](https://doi.org/10.3847/2041-8213/ab91a1)
- Ricci, C., Loewenstein, M., Kara, E., et al. 2021, *ApJS*, 255, 7, doi: [10.3847/1538-4365/abe94b](https://doi.org/10.3847/1538-4365/abe94b)
- Roychowdhury, A. 2023, PhD thesis, University of Maryland Baltimore County
- Ryu, T., Krolik, J., & Piran, T. 2020, *ApJ*, 904, 73, doi: [10.3847/1538-4357/abbf4d](https://doi.org/10.3847/1538-4357/abbf4d)
- Scepi, N., Begelman, M. C., & Dexter, J. 2021, *MNRAS*, 502, L50, doi: [10.1093/mnras/slab002](https://doi.org/10.1093/mnras/slab002)
- Sfaradi, I., Beniamini, P., Horesh, A., et al. 2023, *Monthly Notices of the Royal Astronomical Society*, 527, 7672, doi: [10.1093/mnras/stad3717](https://doi.org/10.1093/mnras/stad3717)
- Shappee, B. J., Prieto, J. L., Grupe, D., et al. 2014, *ApJ*, 788, 48, doi: [10.1088/0004-637X/788/1/48](https://doi.org/10.1088/0004-637X/788/1/48)
- Shepherd, M. C. 1997, in *Astronomical Society of the Pacific Conference Series*, Vol. 125, *Astronomical Data Analysis Software and Systems VI*, ed. G. Hunt & H. Payne, 77
- Shepherd, M. C., Pearson, T. J., & Taylor, G. B. 1994, in *Bulletin of the American Astronomical Society*, Vol. 26, 987–989
- Sobolewska, M., Siemiginowska, A., Migliori, G., et al. 2023, *ApJ*, 948, 81, doi: [10.3847/1538-4357/acbb6c](https://doi.org/10.3847/1538-4357/acbb6c)
- Taylor, G. B., Marr, J. M., Pearson, T. J., & Readhead, A. C. S. 2000, *The Astrophysical Journal*, 541, 112, doi: [10.1086/309428](https://doi.org/10.1086/309428)
- Tonry, J. L., Denneau, L., Heinze, A. N., et al. 2018, *PASP*, 130, 064505, doi: [10.1088/1538-3873/aabadf](https://doi.org/10.1088/1538-3873/aabadf)
- Trakhtenbrot, B., Arcavi, I., MacLeod, C. L., et al. 2019, *ApJ*, 883, 94, doi: [10.3847/1538-4357/ab39e4](https://doi.org/10.3847/1538-4357/ab39e4)
- Tran, H. D., Lyke, J. E., & Mader, J. A. 2011, *ApJ*, 726, L21, doi: [10.1088/2041-8205/726/2/L21](https://doi.org/10.1088/2041-8205/726/2/L21)
- Tremblay, S. E., Taylor, G. B., Ortiz, A. A., et al. 2016, *Monthly Notices of the Royal Astronomical Society*, 459, 820, doi: [10.1093/mnras/stw592](https://doi.org/10.1093/mnras/stw592)
- van Moorsel, G., Kembell, A., & Greisen, E. 1996, in *Astronomical Society of the Pacific Conference Series*, Vol. 101, *Astronomical Data Analysis Software and Systems V*, ed. G. H. Jacoby & J. Barnes, 37
- Wang, Y., Lin, D. N. C., Zhang, B., & Zhu, Z. 2024, *ApJ*, 962, L7, doi: [10.3847/2041-8213/ad20e5](https://doi.org/10.3847/2041-8213/ad20e5)
- Wu, Q. 2009, *MNRAS*, 398, 1905, doi: [10.1111/j.1365-2966.2009.15127.x](https://doi.org/10.1111/j.1365-2966.2009.15127.x)
- Yang, J., van Bemmell, I., Paragi, Z., et al. 2021, *MNRAS*, 502, L61, doi: [10.1093/mnras/slab005](https://doi.org/10.1093/mnras/slab005)
- Zwart, J. T. L., Barker, R. W., Biddulph, P., et al. 2008, *MNRAS*, 391, 1545, doi: [10.1111/j.1365-2966.2008.13953.x](https://doi.org/10.1111/j.1365-2966.2008.13953.x)